Hindawi
Mathematical Problems in Engineering
Volume 2020, Article ID 3918787, 15 pages
https://doi.org/10.1155/2020/3918787

Research Article

Variation of Rock Mass Pressure during Tunnel Construction in Phyllite Stratum

Jianxun Chen,[1] Yanbin Luo,[1] Yao Li,[1] Lijun Chen,[1] Chuanwu Wang,[1] Zeguang Song,[1] and Pengsheng Diao[2]

[1]*School of Highway, Chang'an University, Xi'an 710064, China*
[2]*Shenzhen China Overseas Construction Limited, Shenzhen 518000, China*

Correspondence should be addressed to Yanbin Luo; lyb@chd.edu.cn

Received 18 April 2020; Revised 28 June 2020; Accepted 10 July 2020; Published 11 August 2020

Academic Editor: M. I. Herreros

In this paper, the field monitoring method is used to study the variation of rock mass pressure during the construction of a tunnel in phyllite stratum, and three functions are used to fit and analyze the variation of rock mass pressure with deformation, excavation time, and space. The results show the following (1) When the deformation increases significantly, the rock mass pressure decreases firstly and then increases. This is caused by the insufficient bearing capacity of the rock mass in the arch foot of the supporting structure after the excavation of the upper bench, which leads to a settlement of supporting structure and surrounding rock. (2) Compared with other kinds of fitting functions, the logistic function can better characterize the variation of the pressure of surrounding rock with deformation, excavation time, and distance from the face. This paper provides a reliable reference for the design and construction of the tunnel in phyllite stratum. The logistic function can be used to present and predict the change of rock mass pressure with deformation, excavation time, and space in similar rock mass conditions.

1. Introduction

Rock mass pressure is the pressure acting on supporting structure, and it is caused by deformation or loosening of the surrounding rock after a tunnel is excavated. After the excavation of the tunnel, the initial stress field of the surrounding rock is disturbed, and the rock mass pressure enters the dynamic adjustment stage. In the soft surrounding rock, this stage lasts for a long time, and the stress and deformation of the tunnel are difficult to be stable for a long time, which is not good for the safety and stability of the overall structure of the tunnel [1–3]. Therefore, to assure a safe construction, it is important to study the changing pattern of rock mass pressure during tunnel construction. In recent years, the changing pattern of rock mass pressure during tunnel construction has been studied by analytical method, numerical simulation, on-site monitoring, and laboratory model tests [4–12].

By using the analytical method, many researchers proposed a new method or new coefficient to better predict the change of the rock mass pressure. Panet proposed a load release coefficient to describe the load variation during tunnel construction. It is found that the increase in load is due to the rheological behavior of the rock mass [13]. Guo et al. used a volume loss rate to characterize the variation of tunnel rock mass pressure and found that the volume loss rate and the load release rate in the soil tunnel had a linear relationship [14]. Zhao et al. used analytical and numerical solutions to analyze the lining forces of shallow and deep buried soil tunnels. It is found that different constitutive models of the soil and construction method lead to different rock mass pressure and lining force [8]. The analytical solution method can not consider the complex geological conditions in the process of tunnel construction, so it needs a model test, numerical simulation, and other methods to improve the practical significance of the study.

Model tests are also widely used to analyze the change of rock mass pressure. Li et al. used a comprehensive load release rate to study the load release process of tunnel excavation, results showed that the whole section should be taken as the research object, and the overall load release state of the section should be analyzed [15]. Lei et al. used the

method of model test to systematically study the change laws and distribution forms of structural stress and rock mass pressure of shallow buried tunnels. The results show that the rock mass pressure and structural stress constantly change in the process of tunnel excavation, and the stress release near the excavation face is large, showing unsymmetrical pressure characteristics and time-space effect [16]. Huang et al. studied the failure mechanism of soft rock tunnel under surcharge through the large-scale model test and found that the rock mass pressure is mainly concentrated on the roof of the tunnel rather than the sidewall [17]. Numerical modelling is also widely used to simulate the change of the rock mass pressure, together with the back analysis. Li et al. modeled the stress changes during the construction of a subway tunnel, and results showed that the rock mass pressure near excavation changed significantly until the ring closure was reached [18]. Mark et al. used a finite-element model (FEM) to study the distribution of stress, strain, and deformation during tunnel excavation. And the bearing capacity of pressure tunnels was determined by the superposition principle [9]. Eberhardt researched the near-field stress path in the excavation process with a detailed three-dimensional finite-element model. The results demonstrate that the spatial and temporal evolution of the three-dimensional stress field includes a series of changes of deviatoric stress as well as principal stress axis [19]. Chen et al. studied the change of rock mass pressure during the construction of soft rock tunnel through the combination of field monitoring and numerical simulation and found that the surrounding rock pressure was stable 65 to 70 days after the completion of support structure [20]. The correctness of the analytical solution and model test is verified by numerical simulation, but it is still different from the actual situation in the field. Therefore, field monitoring has a strong practical significance in the process of tunnel research.

On-site monitoring plays an important role in the analysis of rock mass pressure during tunnel construction. Hu et al. found that the horizontal stress of the bias tunnel was over released and the measured pressure value of side walls was much larger than the calculated pressure value by comparing the on-site monitoring data with the theoretical calculation results [21]. Walton et al. used LiDAR scan data for tunnel section analysis and back-calculation. A new ellipse fitting data analysis method is proposed, which can be used to analyze the rock mass pressure distribution of the tunnel section [22]. Kontogianni and Stiros analyzed a large number of records obtained by electronic theodolite in tunnels. It proved that the deformation in tunnels would be affected by the stress release of adjacent parts of the rock mass [23].

In the past, a large number of researchers have obtained the law that the rock mass pressure decreases with the increase of surrounding rock deformation through numerical simulation and theoretical calculation [24–28]. This is different from the change rule that the rock mass pressure increases first and then decreases when the clearance convergence and settlement increase rapidly, which is monitoring under the special geological conditions in this paper. Therefore, further research is needed to provide a theoretical basis for the design and construction of the tunnel. Based on the monitoring of the Mingyazi tunnel, this study analyzes the variation of rock mass pressure with the deformation, time, and distance from excavation face during the construction process of the phyllite tunnel and summarizes a changing pattern.

2. Project Overview

The Mingyazi tunnel is located in Shaanxi province. It is a four-lane two-tunnel expressway project. The left line tunnel is 4949 m, and the right line tunnel is 4985 m. It is an extralong tunnel with a maximum buried depth of 320 m.

The monitoring measurement section is selected according to the field conditions. The right line has 9 deformation monitoring sections, including 1 stress monitoring section, and the station number of the stress monitoring section is YK214 + 011 (hereinafter referred to as 011 section). The main lithology of the monitoring section is gray-black carbon phyllite, with low stability and strength, which is easy to produce creep and be soften in water. It belongs to the grade V weak rock mass segment according to "Technical Specifications for Highway Tunnel Construction" (JTG/TF60-2009) [29]. The surrounding rock conditions of section 011 are shown in Figure 1.

Tunnel construction adopts three-bench and seven-step construction method, and its construction sequence is shown in Figure 2. The construction sequence is to excavate the arc heading (1), left and right sides of the middle bench (2, 3), left and right sides of the lower bench (4, 5), and finally excavate the three parts of reserved core soil (6–1, 6–2, 6–3).

The tunnel is supported by a composite lining. Grouted pipe spiling is used for presupport, the usually used rock bolts are not used, and the feet-lock anchor pipe is installed. The support parameters are shown in Figure 3.

3. In Situ Monitoring

According to the requirements of "Technical Specifications for Highway Tunnel Construction" (JTG/TF60-2009) [29], the monitoring contents and methods of the Mingyazi tunnel are proposed based on its construction methods and geological conditions. In the monitoring of crown settlement and clearance convergence, the noncontact measurement method is used to improve the measurement precision and complete the collection of monitoring data in the field. Monitoring items, instruments, and sensors are summarized in Table 1. The deformation of the monitoring section, the layout of the measuring points, and the numbers of the survey points are shown in Figures 4 and 5.

4. Analysis of Monitoring Results

4.1. Variation of Rock Mass Pressure and Deformation with Time. The relation between the rock mass pressure and settlement of the YK214 + 011 section is shown in Figures 6–10. The relation between rock mass pressure and clearance convergence is shown in Figures 11 and 12. *Yx*

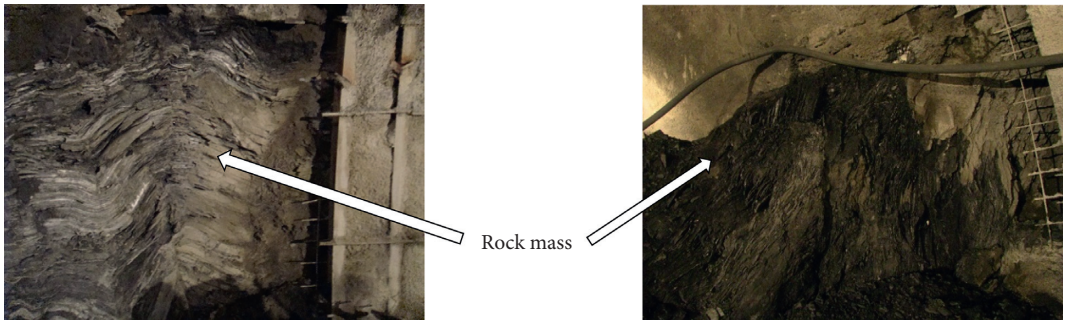

Figure 1: The field geological condition of the Mingyazi tunnel.

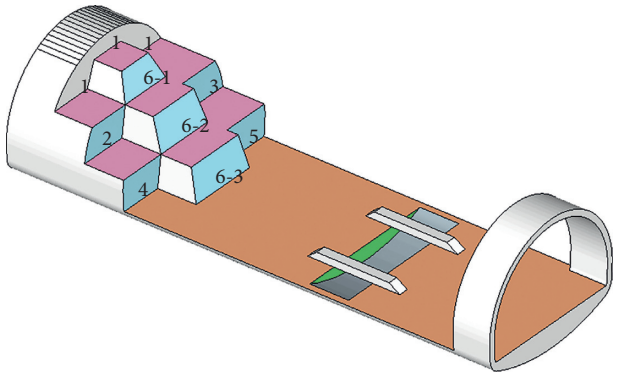

Figure 2: Construction method of the Mingyazi tunnel.

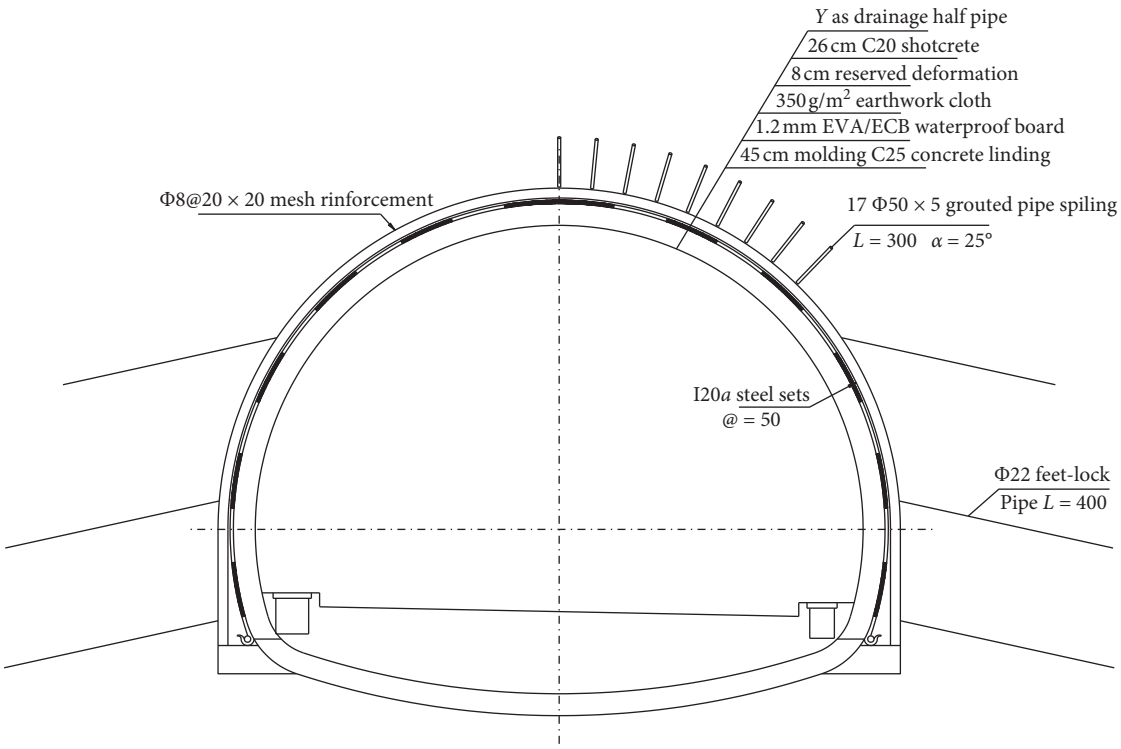

Figure 3: Support parameters of the Mingyazi tunnel.

represents the rock mass pressure at the xth measuring point. For example, $Y0$ represents the rock mass pressure at point 0 of the arch crown in Figure 5.

It can be seen from Figures 6–10 that there is a certain correlation between rock mass pressure and settlement development. In Figures 6 and 7, rock mass pressure

Table 1: On-site monitoring measurement project and method of the Mingyazi tunnel.

Number	Monitoring content	Instrument	Monitoring frequency	
1	Clearance convergence	TOPCON (OS-600G) total station	1–15 days 16 days-1 month 1 month later	1-2 times/day 1 time/day 1-2 times/week
2	Crown settlement	TOPCON (OS-600G) total station	1–15 days 16 days-1 month 1 month later	1-2 times/day 1 time/day 1-2 times/week
3	Rock mass pressure and contact pressure	Pressure sensor	1 time/day	

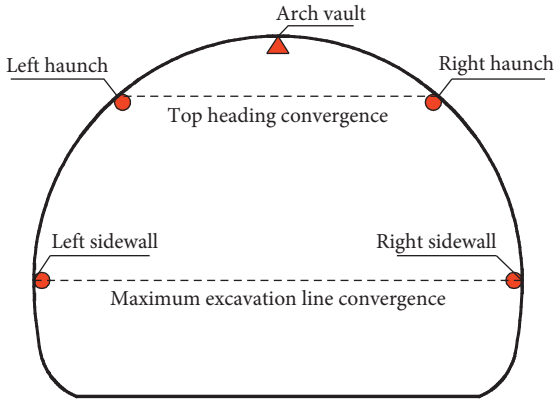

Figure 4: Measured points arrangement of arch settlement and clearance convergence.

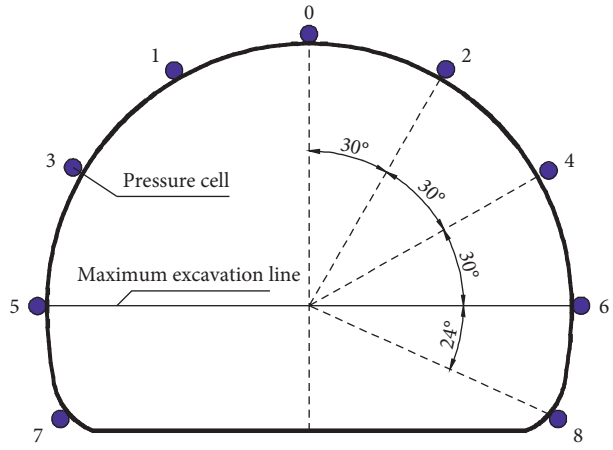

Figure 5: Sensor arrangement for stress monitoring in initial support.

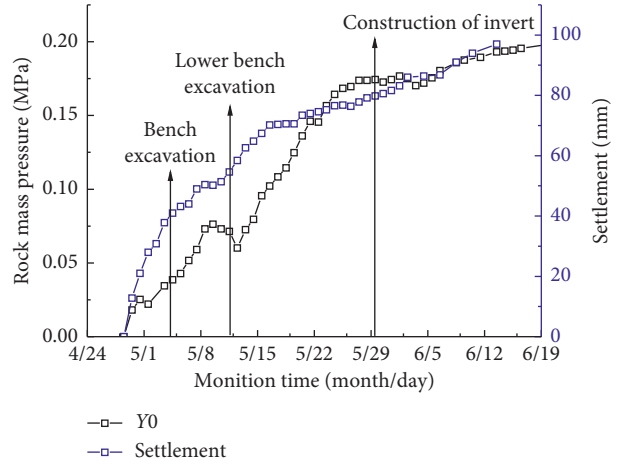

Figure 6: Rock mass pressure and settlement curve of *Y*0.

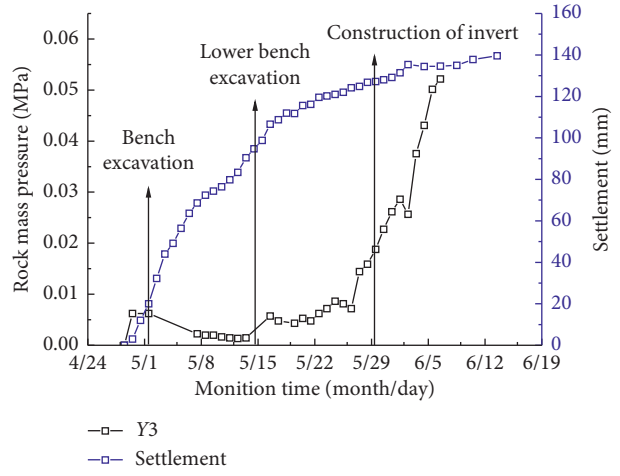

Figure 7: Rock mass pressure and settlement curve of *Y*3.

increases with the crown settlement, but the increasing rate of rock mass pressure is different at *Y*0 and *Y*3. In Figures 8–10, while the settlement is accumulated, rock mass pressure increases first, followed by a decrease and increase again. It can be concluded that rock mass pressure generally increases with the increasing crown settlement. However, in Figures 9 and 10, the excavation of the lower bench results in a sharp decrease of the rock mass pressure, which is because the excavation of the lower bench causes the stress in the surrounding rock to release with the increase of deformation.

Figures 11 and 12 show the changes in rock mass pressure and convergence. It can be seen that convergence is significantly accumulated mostly after the construction of middle bench (noted by bench excavation in the figures), while the rock mass pressure is accumulated mostly after the construction of the lower bench.

4.2. Variation of Rock Mass Pressure with Time. The rock mass pressure monitoring results of the YK214 + 011 section and the proportion of the rock mass pressure variation at

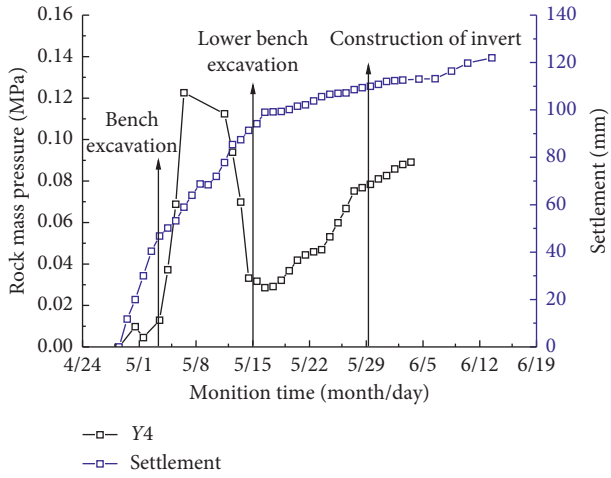

Figure 8: Rock mass pressure and settlement curve of *Y*4.

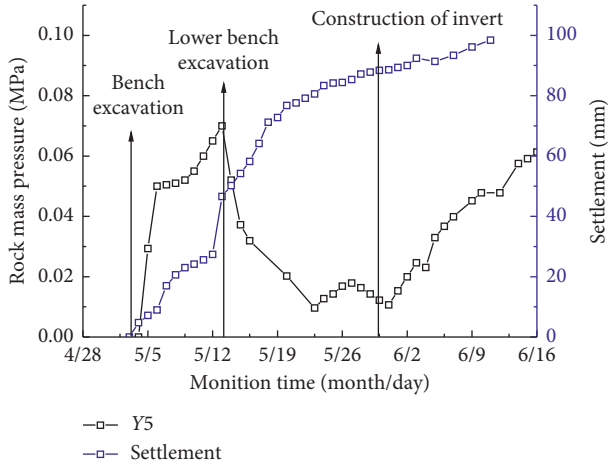

Figure 9: Rock mass pressure and settlement curve of *Y*5.

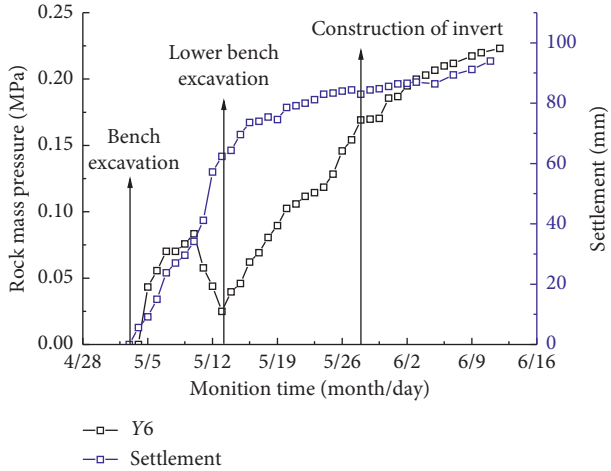

Figure 10: Rock mass pressure and settlement curve of *Y*6.

each stage to the final measured values are shown in Table 2. The relationship between rock mass pressure and time is shown in Figure 13, and the distribution of rock mass pressure is shown in Figure 14.

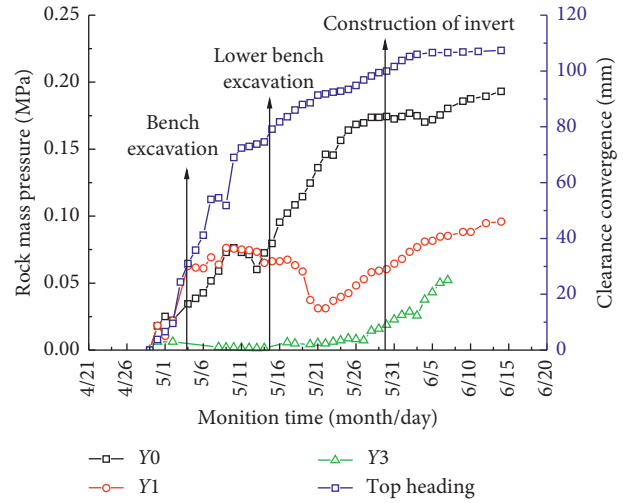

Figure 11: Rock mass pressure of arch and clearance convergence curve of top heading.

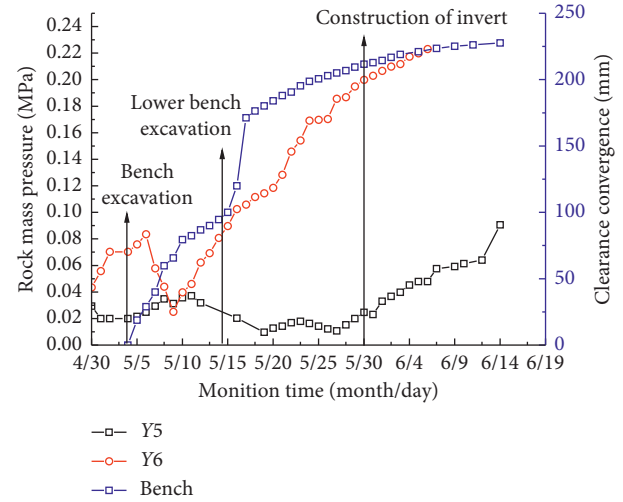

Figure 12: Rock mass pressure of sidewalls and clearance convergence curve of the upper bench.

The average changing ratio of rock mass pressure in the construction stages of the arch and sidewalls in this section are shown in Figure 15.

It can be seen from Figure 13 that after the construction of the upper bench, rock mass pressure at the crown (*Y*0) increases fast, and the rock mass pressure at sidewalls (*Y*4, *Y*5, *Y*6) increases faster. And in Figure 14, the final rock mass pressure at *Y*0 and Y6 points is relatively high. This is due to the fact that the upper bench is located at the maximum excavation line; as a result, the construction of the middle bench has the greatest influence on rock mass, which causes the dramatic increase of the rock mass pressure at the crown and the sidewalls. At this stage, the variation of the rock mass pressure at the sidewalls accounts for 33% of the final monitored value, as shown in Figure 15(b). Figure 15(a) shows that after top heading is excavated, rock mass pressure at crown accumulated 32% of its final monitored value, and rock mass pressure at the crown (*Y*0) changes rapidly as shown in Figure 13.

Table 2: Monitoring results of rock mass pressure in YK214 + 011 section/MPa.

Monitoring positions	Before upper bench excavation		Before lower bench excavation		Before the construction of invert		Before the construction of the secondary lining		Final monitoring value
	Rock mass pressure	Ratio (%)	Rock mass pressure	Ratio (%)	Rock mass pressure	Ratio (%)	Rock mass pressure	Ratio (%)	
*Y*0	0.034	17	0.080	39	0.174	84	0.196	95	0.206
*Y*1	0.063	54	0.066	57	0.060	52	0.100	86	0.116
*Y*2	—	—	—	—	—	—	—	—	—
*Y*3	0.013	25	0.015	29	0.019	37	0.052	100	0.052
*Y*4	0.003	3	0.033	37	0.078	88	0.089	100	0.089
*Y*5	—	—	0.037	40	0.012	13	0.064	69	0.093
*Y*6	—	—	0.046	21	0.170	76	0.223	100	0.223
*Y*7	—	—	—	—	—	—	0.065	155	0.042
*Y*8	—	—	—	—	—	—	—	—	—

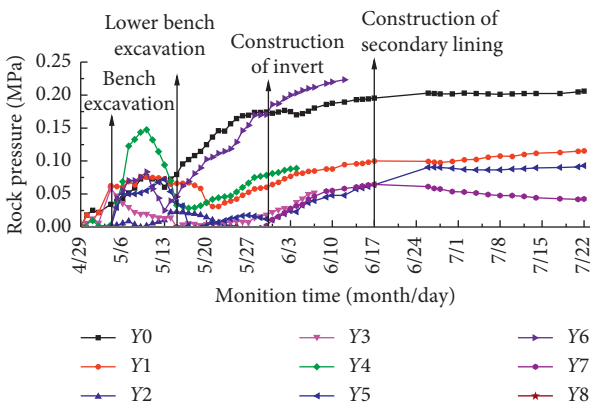

Figure 13: Temporal curve of rock mass pressure in YK214 + 011 section.

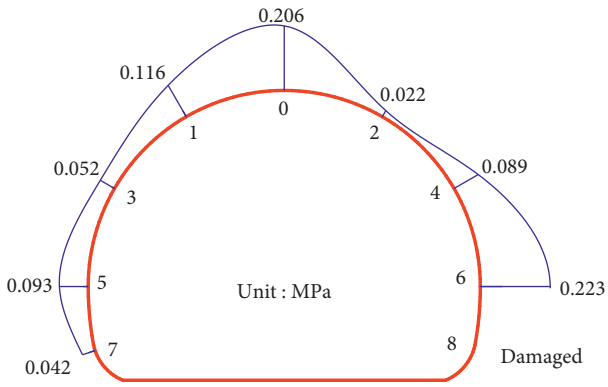

Figure 14: Distribution of rock mass pressure.

It is interesting to note that after the construction of the upper bench and before the construction of the lower bench, the rock mass pressure at each part suddenly drops at the same time. This is caused by the insufficient support of rock mass at skewback (bottom of the constructed sidewalls). Due to the limited bearing capacity, supporting structure, and the rock mass move downwards together. As a result, after experiencing the deformation, rock mass pressure is decreased, and the loose rock mass around the tunnel becomes larger followed by further compaction of rock mass with rock mass pressure increase.

Figure 13 also shows that after the excavation of the lower bench, rock mass pressure increases relatively fast, but the change rate decreases gradually, especially after the installation of the secondary lining. From Figure 15, it can be seen that excavation of the lower bench has little effect on the increase of rock mass pressure at the arch, but has a greater influence on the increase of rock mass pressure at sidewalls which accounts for 31% of the final monitored value. Before the construction of invert, the rock mass pressure at the crown and the sidewalls accumulated more than 65% of the final monitoring value. It should be noted that before secondary lining is installed, the rock mass pressure reaches a relative steady state, and the state extends after the construction of the secondary lining.

4.3. Relation between Rock Mass Pressure and Distance to Excavation Face. The change of rock mass pressure with distance to excavation face is shown in Figure 16. In Figure 16, D represents the maximum excavation diameter of the tunnel. For the Mingyazi tunnel, D is about 12.3 m. In tunnel engineering, the rock mass pressure at certain section is greatly influenced by both after excavation time and distance to excavation face. Therefore, it is important to analyze the relation between rock mass pressure with the distance to excavation face. In the construction process of the YK214 + 011 section, the excavation speed was basically the same, and there was no delay during construction. The progress was about 2 m/day. As a result, the time effect in the process can be considered unchanged.

From Figure 16, we can see the following: (1) When the distance from the excavation surface is within 1-time tunnel diameter, the rock mass pressure changes rapidly. This is mainly due to the fact that the monitoring section is close to the excavation face, where there is a great disturbance to the nearby rock mass. (2) When the distance is between 1 and 2.5 times of tunnel diameter, the rock mass pressure drastically fluctuates, which is caused by the complex and long construction process.

4.4. Fitting Analysis of Variation Law of Rock Mass Pressure. The relation between rock mass pressure and distance to excavation face is found in Figure 16. However, the data of

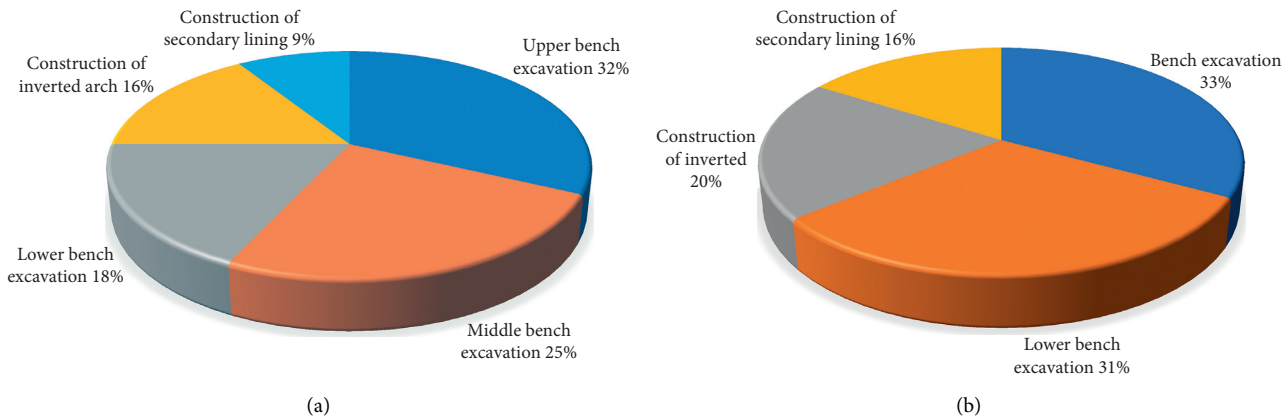

Figure 15: (a) Proportion of rock mass pressure changes in the arch. (b) Proportion of rock mass pressure changes on sidewalls.

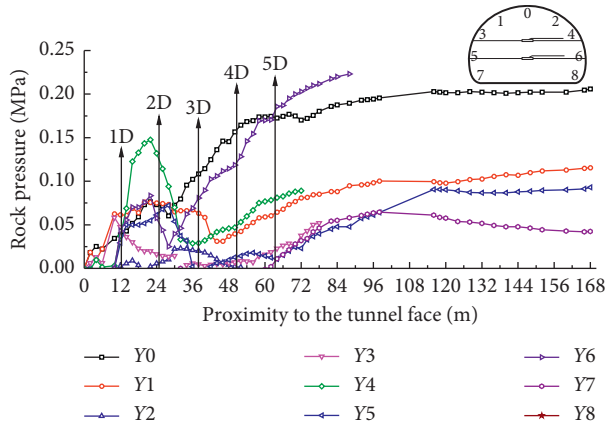

Figure 16: Space curve of rock mass pressure in YK214 + 011 section.

deformation, excavation time, and distance from the face are relatively obtained data. Therefore, if one correlation function can characterize the pressure of rock mass with the changing deformation, excavation time, and distance from the tunnel face, the development of rock mass pressure can be predicted accordingly.

Taking the YK214 + 011 section of the Mingyazi tunnel as an example, the relationship between the rock mass pressure and deformation, excavation time, and distance from the tunnel face is analyzed. Origin data analysis software is used to fit and analyze the rock mass pressure. In the analysis, logarithmic function, sigmoid function, and multiple functions are used to fit the data, and the optimal function is finally selected to characterize the variation of rock mass pressure. The logistic function is adopted to formulate the S-type function, and multifunction uses the cubic formulation to represent. The basic forms of the functions are shown in equation (1)–(3). In the three fitting formulas, y represents rock pressure, x represents settlement, and the other symbols are variable parameters as shown in Table 3:

$$y = a - b\ln^{(x+c)}, \tag{1}$$

$$y = \frac{A_1 - A_2}{1 + (x/x_0)^p} + A_2, \tag{2}$$

$$y = A + Bx + Cx^2 + Dx^3. \tag{3}$$

4.5. Fitting Analysis of Variation of Rock Mass Pressure with Deformation. Fitting is performed on the change of rock mass pressure with settlement and clearance convergence at the YK214 + 011 section. The representative fitting results are selected, as shown in Figures 17–19, with the fitting correlation coefficients in the three functions for each monitoring point listed in Tables 4 and 5, and the range of each function constant is, respectively, listed in Tables 3 and 6.

It can be seen from Tables 3–6 that except the left sidewalls (measurement point No. 5), the correlation coefficients of the fitting results in all points are very high, and the values are all above 0.7, among which the correlation coefficient by the logistic function is the highest. At the same time, it can be seen that the correlation coefficient obtained by fitting the logarithmic function is generally low. Therefore, under the condition of two-lane V-class rock mass, the logarithmic function cannot characterize the change of rock mass pressure with deformation. In addition, although the R^2 by the cubic function fitting is very high, the fitting curve finally appears as a rising or falling trend, which is not consistent with the reality, so the multiple functions cannot

Table 3: Fitting parameter range of rock mass pressure and settlement.

Function types	Basic form	Parameters	Value range
Logarithmic function	$y = a - b\ln^{(x+c)}$	a	−10.127~0.045
		b	−1.184~0.005
		c	2941.362~5151.256
Logistic function	$y = ((A_1 - A_2)/(1 + (x/x_0)^P)) + A_2$	A_1	0.003~0.027
		A_2	0.046~0.241
		x_0	56.413~82.275
		P	18.718~23.257
Multiple functions	$y = A + Bx + Cx^2 + Dx^3$	A	−0.007~0.019
		B	−0.002~0.006
		C	−0.0002~0.0001
		D	−0.002~0.001

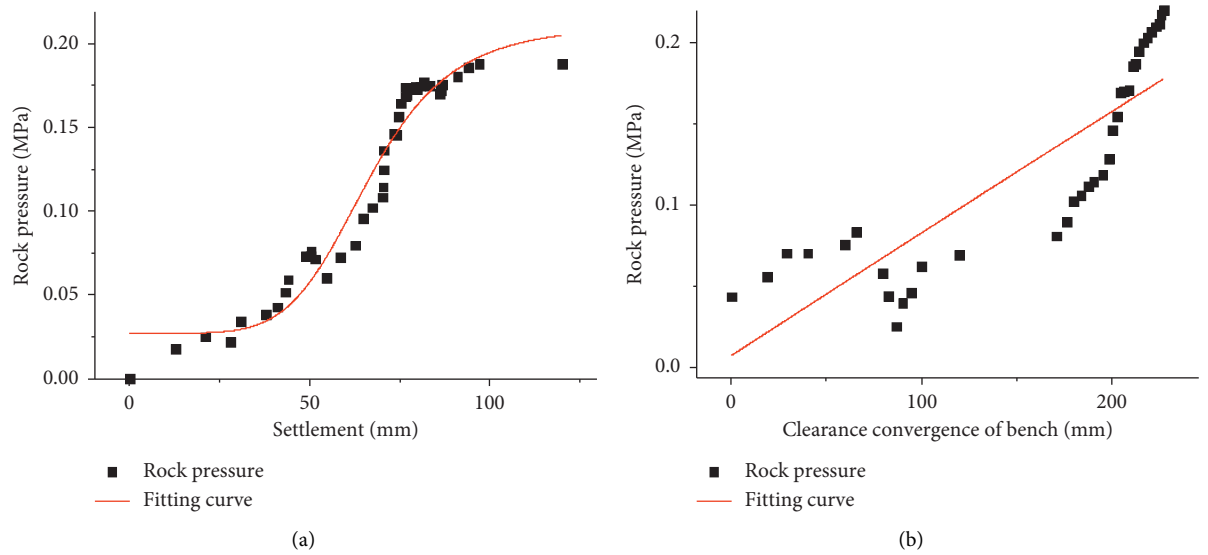

Figure 17: Logarithmic function fitting results. (a) Fitting results of rock mass pressure and settlement (*Y*0). (b) Fitting results of rock mass pressure and clearance convergence (*Y*6).

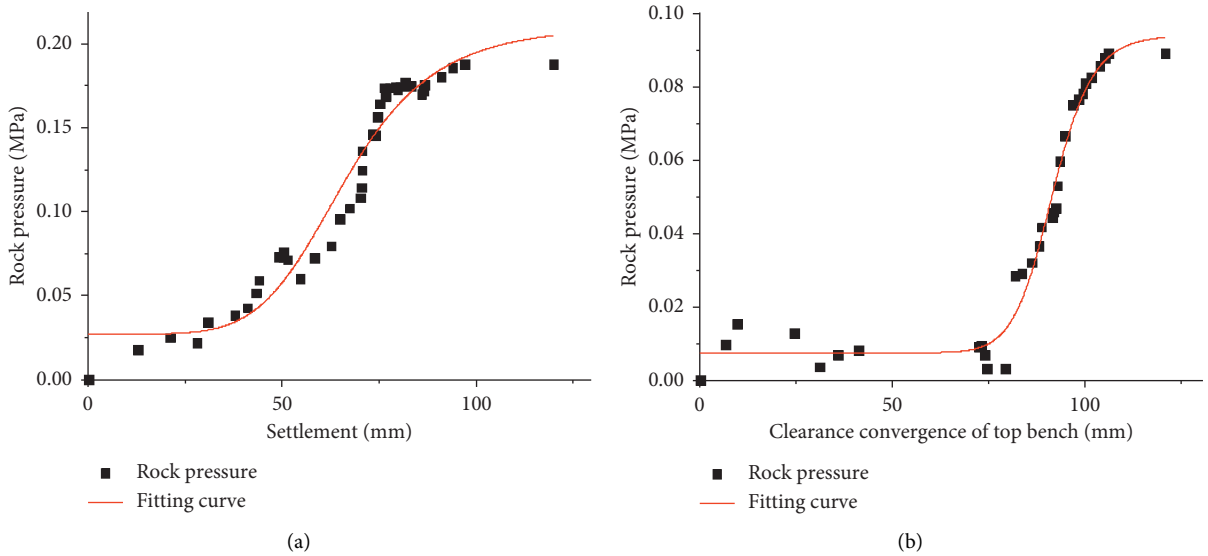

Figure 18: Logistic function fitting results. (a) Fitting results of rock mass pressure and settlement (*Y*0). (b) Fitting results of rock mass pressure and clearance convergence (*Y*6).

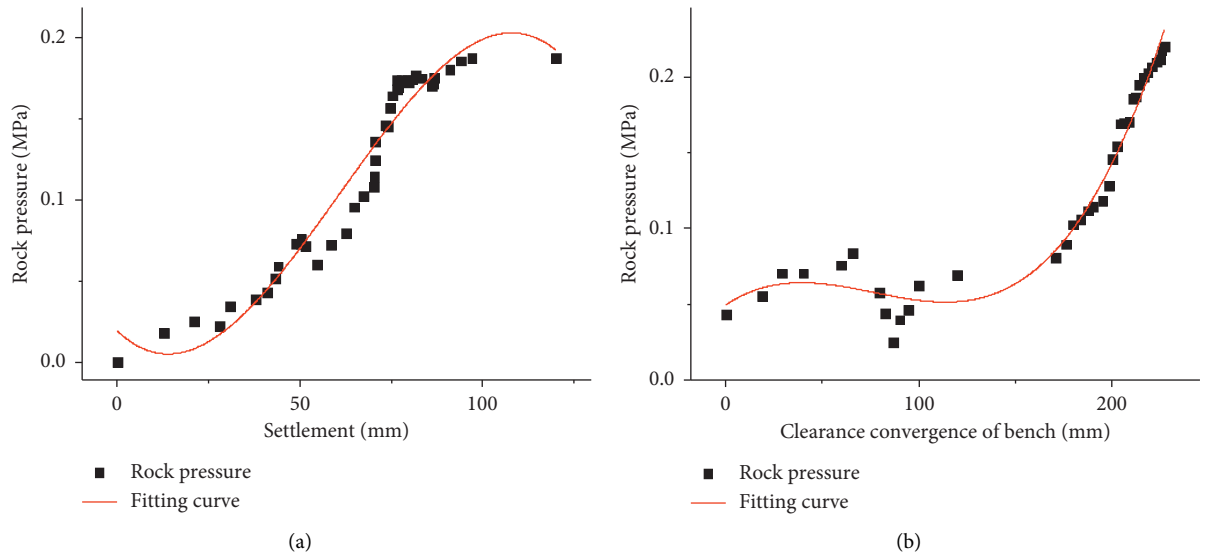

Figure 19: Multiple function fitting results. (a) Fitting results of rock mass pressure and settlement (*Y0*). (b) Fitting results of rock mass pressure and clearance convergence (*Y6*).

Table 4: Fitting correlation coefficient between rock mass pressure and settlement.

Function types	Results	*Y0*	*Y3*	*Y4*	*Y5*	*Y6*
Logarithmic function	Correlation coefficient R^2	0.764	0.285	0.370	0.013	0.546
Logistic function	Correlation coefficient R^2	0.946	0.949	0.974	0.064	0.929
Multiple functions	Correlation coefficient R^2	0.941	0.868	0.965	0.619	0.932

Table 5: Fitting correlation coefficient between rock mass pressure and clearance convergence.

Function types	Results	*Y3*	*Y4*	*Y5*	*Y6*
Logarithmic function	Correlation coefficient R^2	0.259	0.534	0.071	0.713
Logistic function	Correlation coefficient R^2	0.948	0.975	0.103	0.968
Multiple functions	Correlation coefficient R^2	0.848	0.832	0.375	0.968

Table 6: Fitting parameter range of rock mass pressure and clearance convergence.

Function types	Basic form	Parameters	Value range
Logarithmic function	$y = a - b\ln^{(x+c)}$	a	−52.749~−10.081
		b	−5.891~−1.205
		c	3654.005~7747.978
Logistic function	$y = ((A_1 - A_2)/(1 + (x/x_0)^p)) + A_2$	A_1	0.003~0.007
		A_2	0.094~0.276
		x_0	177.585~206.915
		P	15.085~17.577
Multiple functions	$y = A + Bx + Cx^2 + Dx^3$	A	0.002~0.050
		B	−0.001~0.001
		C	−0.00002~0.00001
		D	−0.0002~0.0002

be used to characterize the relationship between pressure and deformation of the rock mass. From the range of constant terms, the value in the logarithmic function is discrete, while the value in logistic function and multiple functions fluctuates little.

Considering the above factors, the fitting trend of logistic function with a higher correlation coefficient is more consistent with the measured data, and it has the minimum fluctuation of the constant range in characterizing the variation of rock mass pressure with deformation.

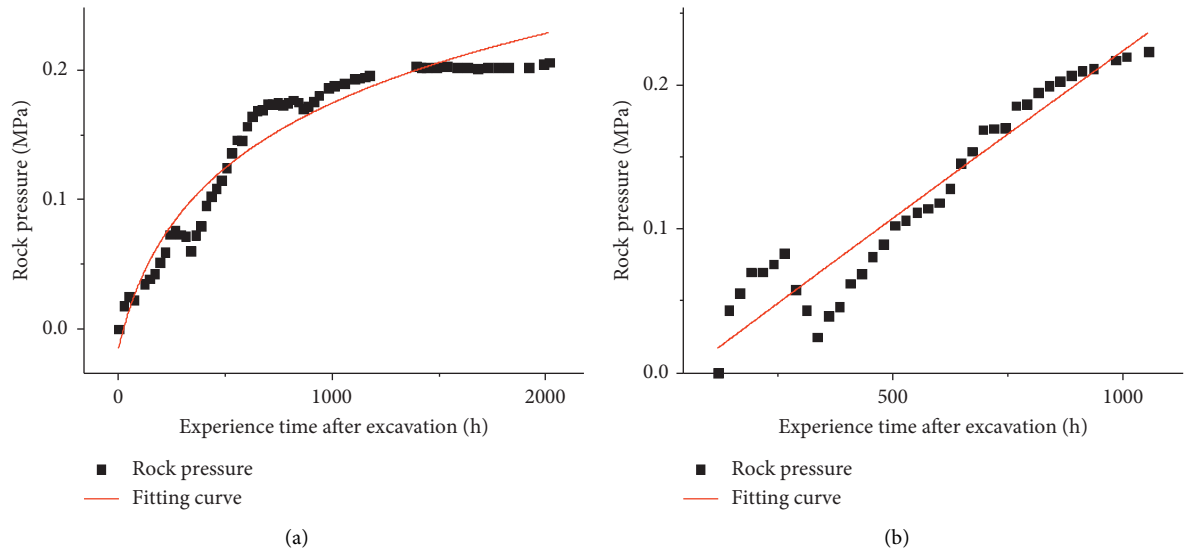

Figure 20: Logarithmic function fitting result. (a) Logarithmic function fitting result (*Y*0). (b) Logarithmic function fitting result (*Y*6).

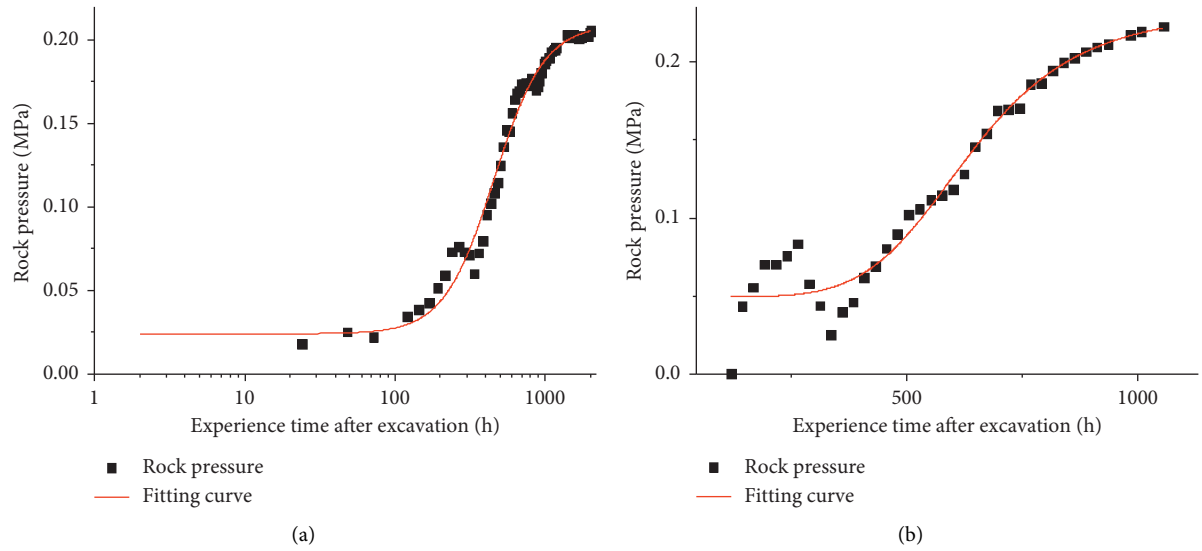

Figure 21: Logistic function fitting result. (a) Logistic function fitting result (*Y*0). (b) Logistic function fitting result (*Y*6).

4.6. Fitting Analysis of the Variation of Rock Mass Pressure with Time. Representative fitting curves of the change of rock mass pressure with excavation time at YK214 + 011 section are shown in Figures 20–22, the fitting correlation coefficient of each point by using three functions is shown in Table 7, and the range of each function constant is shown in Table 8.

It can be seen from Table 7 that the correlation coefficient between rock mass pressure and excavation time is high except for the right arch foot (point No. 4). Most correlation coefficients are greater than 0.7, and the correlation coefficient of the logistic function is the highest among the three functions. At the same time, it can be seen that the fitting curves of multiple functions are still increasing or decreasing at last, which is obviously not consistent with the actual situation. Therefore, multiple functions cannot be used to characterize the change of rock mass pressure and excavation time. From the value range of constant term, the value range of the logarithm function is larger compared with that of the logistic function.

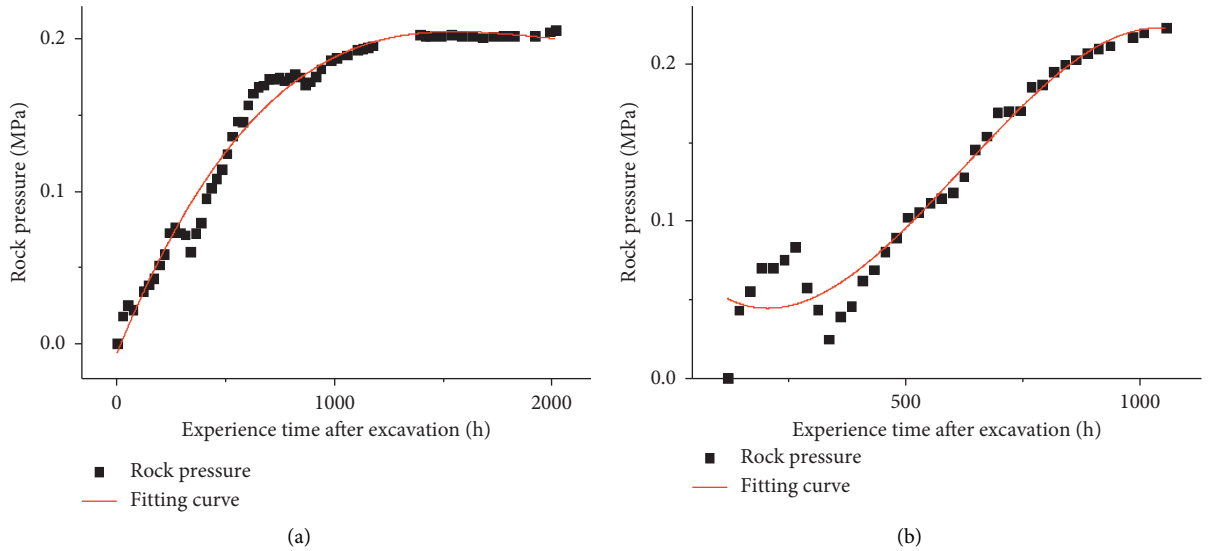

Figure 22: Multiple function fitting result. (a) Multiple function fitting result (*Y*0). (b) Multiple function fitting result (*Y*6).

Table 7: Correlation coefficient between rock mass pressure and excavation time.

Function types	Results	*Y*0	*Y*3	*Y*4	*Y*5	*Y*6
Logarithmic function	Correlation coefficient R^2	0.931	0.538	0.067	0.478	0.911
Logistic function	Correlation coefficient R^2	0.982	0.796	0.323	0.704	0.952
Multiple functions	Correlation coefficient R^2	0.975	0.826	0.425	0.742	0.942

Table 8: Range of parameters for rock mass pressure and excavation time.

Function types	Basic form	Parameters	Value range
Logarithmic function	$y = a - b\ln^{(x+c)}$	a	−52.439~0.017
		b	−5.248~−0.084
		c	−24~119.254
Logistic function	$y = ((A_1 - A_2)/(1 + (x/x_0)^P)) + A_2$	A_1	0.014~0.026
		A_2	0.021~0.233
		x_0	456.969~638.652
		P	5.339~11.030
Multiple functions	$y = A + Bx + Cx^2 + Dx^3$	A	−0.006~0.086
		B	−0.0004~0.0004
		C	−0.00001~0.00002
		D	−0.00002~0.00005

In general, the quality of the fitting function needs to consider three factors: the correlation coefficient R^2, the trend of the fitting curve and the value range of each function constant. The logistic function has the highest correlation coefficient, the best fit with data, and the range of value fluctuates little. As a result, it is recommended to use the logistic function to characterize the change of rock mass pressure with excavation time.

4.7. Fitting Analysis of the Change of Rock Mass Pressure with Distance to Excavation Face. The change of rock mass pressure with distance from the tunnel face is fitted and analyzed. The representative fitting results of each function are selected as shown in Figures 23–25. The correlation coefficients obtained by the fitting are recorded in Table 9, and the range of the value of each function constant item is recorded in Table 10.

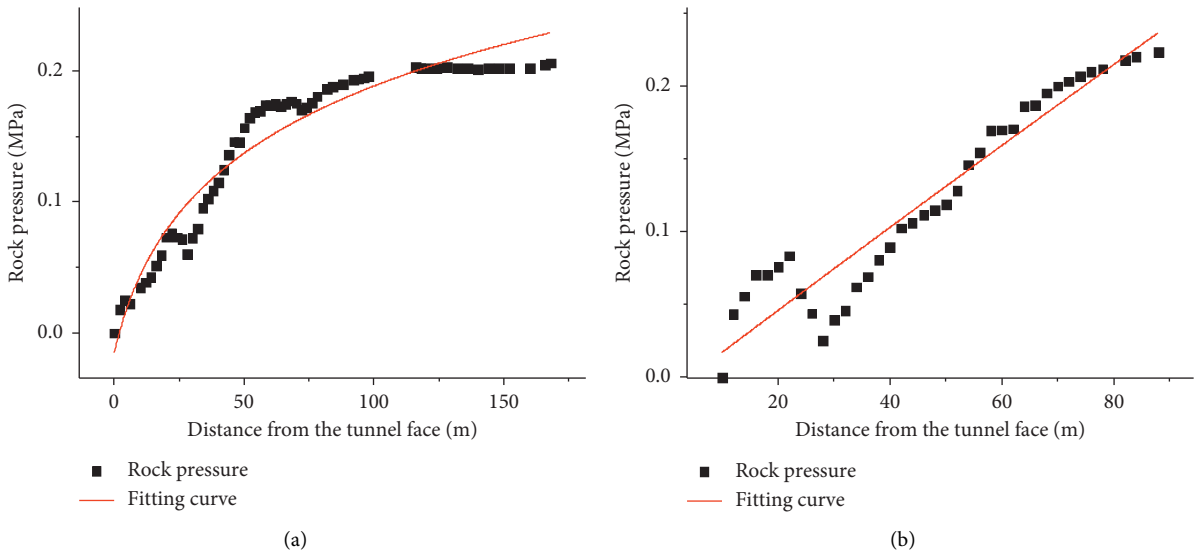

Figure 23: Logarithmic function fitting result. (a) Logarithmic function fitting result (*Y*0). (b) Logarithmic function fitting result (*Y*6).

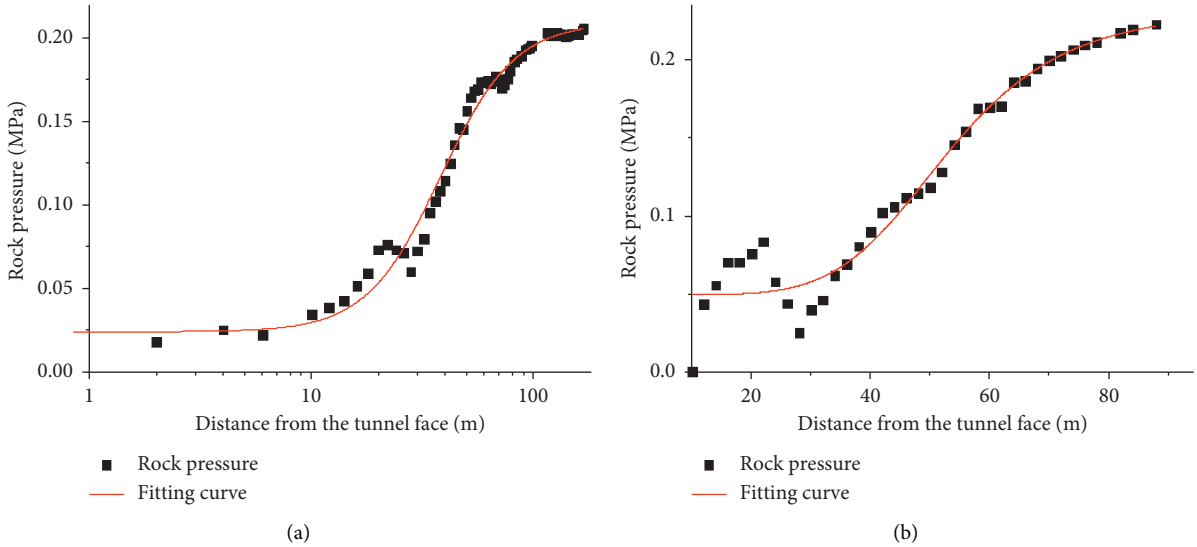

Figure 24: Logistic function fitting result. (a) Logistic function fitting result (*Y*0). (b) Logistic function fitting result (*Y*6).

It can be seen from Table 9 that the correlation coefficient between rock mass pressure and distance from excavation face is high except for the right arch foot (point No. 4). Most correlation coefficient are greater than 0.7, among them, the logistic function has the highest correlation coefficient. At the same time, it can be seen that the fitting curve obtained by multiple functions is inconsistent with the measured data. Therefore, multiple functions cannot be used to characterize the spatial variation of rock mass pressure. From the value range of each function constant term, it can be concluded that the value range of the logarithm function is wide, and the value range of the logistic function is relatively concentrated.

Considering above factors, when the logistic function is used to characterize the change of the rock mass pressure and the distance from the tunnel face, the correlation coefficient is higher, the trend of the fitting curve is more consistent with the actual situation, and the range of each constant term is easier to be determined.

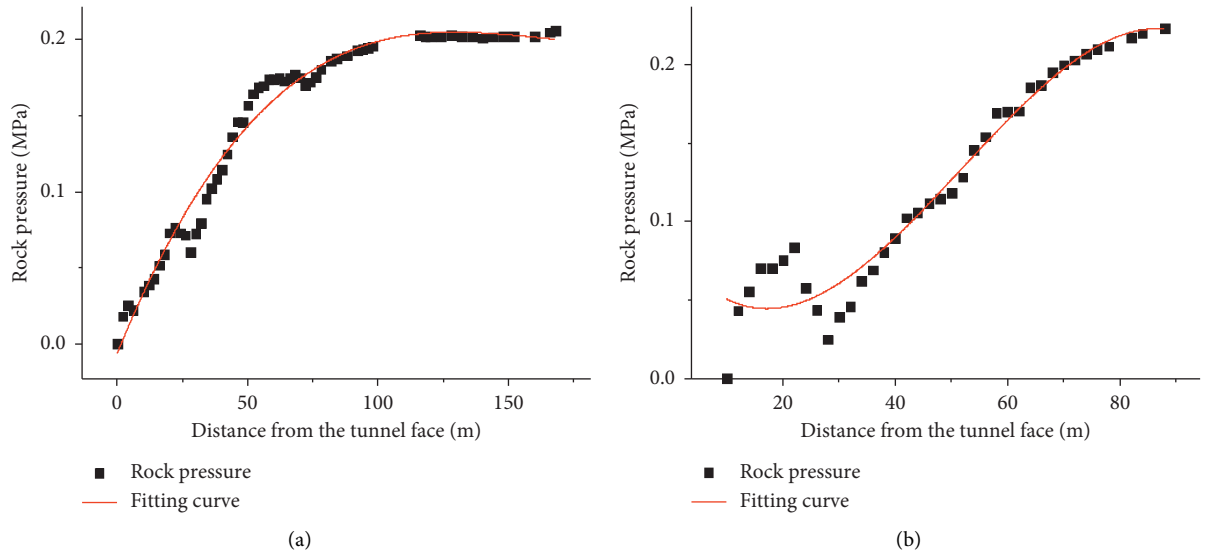

Figure 25: Multiple function fitting result. (a) Multiple function fitting result (*Y*0). (b) Multiple function fitting result (*Y*6).

Table 9: Fitting correlation coefficient between rock mass pressure and distance from the tunnel face.

Function types	Results	*Y*0	*Y*3	*Y*4	*Y*5	*Y*6
Logarithmic function	Correlation coefficient R^2	0.931	0.737	0.067	0.468	0.910
Logistic function	Correlation coefficient R^2	0.982	0.764	0.323	0.711	0.952
Multiple functions	Correlation coefficient R^2	0.975	0.837	0.425	0.737	0.941

Table 10: Range of fitting parameters of rock mass pressure and distance from the tunnel face.

Function types	Basic form	Parameters	Value range
Logarithmic function	$y = a - b\ln^{(x+c)}$	a	−31.034~0.019
		b	−4.255~−0.001
		c	1465.809~4976.583
Logistic function	$y = ((A_1 - A_2)/(1 + (x/x_0)^P)) + A_2$	A_1	0.024~0.049
		A_2	0.090~0.233
		x_0	38.081~58.231
		P	2.600~5.339
Multiple functions	$y = A + Bx + Cx^2 + Dx^3$	A	−0.006~0.086
		B	−0.005~0.004
		C	−0.0001~0.0002
		D	−0.0003~0.0003

5. Conclusion

In this paper, based on the measured rock mass pressure at the Mingyazi tunnel, the change of rock mass pressure in the construction process with tunnel deformation, construction process, excavation time, and distance from the tunnel face is analyzed. The following conclusions are obtained:

(1) The increase of rock mass pressure and deformation is inconsistent. When the clearance convergence and settlement experience a rapid growth, the rock mass pressure appears to increase first and then decrease. This is caused by the insufficient bearing capacity of the rock mass in the arch foot of the supporting structure after the excavation of the upper bench, which leads to a settlement of supporting structure and surrounding rock.

(2) During construction, the rock mass pressure is mostly 0.05~0.23 MPa and changed slowly. After each process, the rock mass pressure adjustment time is long and reaches stable about 15 days after the secondary lining installation. It takes 65 to 70 days for the tunnel to stabilize after excavation and support.

(3) In the process of each construction stage, the change proportion of rock mass pressure is relatively

uniform. When the supporting structure gets a full ring closure, the proportion of the rock mass pressure change value at each part accounted for 65% of the final monitoring value.

(4) Under construction, the space effect of the tunnel face is very significant. In the process of tunnel excavation, due to the constraints of the excavation surface, the surrounding rock cannot immediately release all the instantaneous elastic displacement, which is called the "space effect" of the excavation surface. When the test section is within two times of the diameter of the tunnel, the rock mass pressure is significantly affected by the excavation of the tunnel face. The spatial impact range is within three times the diameter of the tunnel (37 m), and the rheological properties of the rock mass dominate the changes afterwards. In view of the influence of rock rheological properties on rock pressure, further research is still needed.

(5) The logarithmic function, logistic function, and multiple functions are used to fit and analyze the relationship between rock mass pressure, deformation, excavation time, and distance from the tunnel face. It is found that the R^2 of the logistic function is generally greater than 0.9, which shows that the fitting curve is the most consistent with the actual data and has a better fitting effect. Therefore, it is proposed to use the logistic function to express and predict the change of rock mass pressure during the construction of the phyllite stratum tunnel so as to ensure the safe construction of the tunnel.

Data Availability

The data used to support the findings of this study are included within the article.

Conflicts of Interest

The authors declare no conflicts of interest.

Acknowledgments

This research was funded by the National Key R&D Program of China (Grant no. 2018YFB1600100), the Key Project of National Natural Science Foundation of China (Grant no. 41831286), the Youth Project of National Natural Science Foundation of China (Grant nos. 51908052 and 51808049), Natural Science Foundation of Shaanxi Province (Grant no. 211421190347), and the Fundamental Research Funds for the Central Universities of Ministry of Education of China (Grant no. 300102210216). These supports are gratefully acknowledged.

References

[1] J. X. Chen, W. W. Liu, L. J. Chen et al., "Failure mechanisms and modes of tunnels in monoclinic and soft-hard interbedded rocks: a case study," *KSCE Journal of Civil Engineering*, vol. 24, no. 4, 2020.

[2] W. W. Liu, J. X. Chen, L. J. Chen, Y. B. Luo, Z. Shi, and Y.F. Wu, "Nonlinear deformation behaviors and a new approach for the classification and prediction of large deformation in tunnel construction stage: a case study," *European Journal of Environmental and Civil Engineering*, 2020.

[3] J. L. Qiu, Y. Q. Lu, J. X. Lai, C. X. Guo, and K. Wang, "Failure behavior investigation of loess metro tunnel under local-high-pressure water environment," *Engineering Failure Analysis*, vol. 115, Article ID 104631, 2020.

[4] G. Galli, A. Grimaldi, and A. Leonardi, "Three-dimensional modelling of tunnel excavation and lining," *Computers and Geotechnics*, vol. 31, no. 3, pp. 171–183, 2004.

[5] H. Duddeck, "Application of numerical analyses for tunnelling," *International Journal for Numerical and Analytical Methods in Geomechanics*, vol. 15, no. 4, pp. 223–239, 1991.

[6] Y. Luo, J. Chen, P. Huang, M. Tang, X. Qiao, and Q. Liu, "Deformation and mechanical model of temporary support sidewall in tunnel cutting partial section," *Tunnelling and Underground Space Technology*, vol. 61, pp. 40–49, 2017.

[7] V. Kontogianni, P. Psimoulis, and S. Stiros, "What is the contribution of time-dependent deformation in tunnel convergence?," *Engineering Geology*, vol. 82, no. 4, pp. 264–267, 2006.

[8] C. Zhao, A. Alimardani Lavasan, T. Barciaga, C. Kämper, P. Mark, and T. Schanz, "Prediction of tunnel lining forces and deformations using analytical and numerical solutions," *Tunnelling and Underground Space Technology*, vol. 64, pp. 164–176, 2017.

[9] T. D. Y. F. Mark, M. Marence, A. E. Mynett, and A. J. Schleiss, "Pressure tunnels in non-uniform in situ stress conditions," *Tunnelling and Underground Space Technology*, vol. 42, pp. 227–236, 2014.

[10] J. Litwiniszyn, "Application of the equation of stochastic processes to mechanics of loose bodies," *Archives of Mechanics*, vol. 8, no. 4, pp. 393–411, 1956.

[11] J. X. Chen, Z. L. Xu, Y. B. Luo, J. K. Song, W. W. Liu, and F. F. Dong, "Application of the upper-bench CD method in super large-span and shallow tunnel: a case study of Letuan Tunnel," *Advances in Civil Engineering*, vol. 2020, p. 16, Article ID 8826232, 2020.

[12] Y. B. Luo, Z. Shi, J. X. Chen et al., "Study of deformation behaviors and mechanical properties of central diaphragm in a large-span loess tunnel by the upper bench CD method," *Advances in Civil Engineering*, vol. 2020, p. 16, Article ID 8887040, 2020.

[13] M. Panet, "Time-dependent deformations in underground works," in *Proceedings of the 4th ISRM Congress*, Montreux, Switzerland, September 1979.

[14] R. Guo, Y. Fang, and C. He, "Study on the correlation between stress release and displacement release during tunnel excavation," *Journal of Railway Engineering*, vol. 27, no. 9, pp. 46–50, 2010.

[15] S. C. Li, Y. Zhao, and L. P. Li, "Study of construction section comprehensive load releasing process of ultra-large section railway tunnel," *Rock and Soil Mechanics*, vol. 32, no. 9, pp. 2845–2851, 2011.

[16] M. Lei, L. Peng, and C. Shi, "Model test to investigate the failure mechanisms and lining stress characteristics of shallow buried tunnels under unsymmetrical loading," *Tunnelling and Underground Space Technology*, vol. 46, pp. 64–75, 2015.

[17] F. Huang, C. Wu, B.-A. Jang, Y. Hong, N. Guo, and W. Guo, "Instability mechanism of shallow tunnel in soft rock

subjected to surcharge loads," *Tunnelling and Underground Space Technology*, vol. 99, Article ID 103350, 2020.

[18] D. Y. Li, Z. X. Xu, and L. J. Wang, "Numerical simulation analysis of the combined system of the initial support of the underground tunnel," *Railway Engineering*, vol. 34, no. 5, pp. 34–37, 2007.

[19] E. Eberhardt, "Numerical modelling of three-dimension stress rotation ahead of an advancing tunnel face," *International Journal of Rock Mechanics and Mining Sciences*, vol. 38, no. 4, pp. 499–518, 2001.

[20] J. Chen, Y. Luo, Y. Li, P. Zhao, D. Xu, and Q. Wang, "The change of rock mass pressure of Lianchengshan tunnel," *Environmental Earth Sciences*, vol. 79, no. 9, 2020.

[21] J. C. Hu, F. Y. Sun, Y. Li, L. Cui, and M. J. Ji, "On-site monitoring and comparative analysis about surrounding rock pressure variation with time in unsymmetrical loading tunnel," *Earth and Environmental Science*, vol. 295, pp. 42–51, 2019.

[22] G. Walton, D. Delaloye, and M. S. Diederichs, "Development of an elliptical fitting algorithm to improve change detection capabilities with applications for deformation monitoring in circular tunnels and shafts," *Tunnelling and Underground Space Technology*, vol. 43, pp. 336–349, 2014.

[23] V. A. Kontogianni and S. C. Stiros, "Induced deformation during tunnel excavation: evidence from geodetic monitoring," *Engineering Geology*, vol. 79, no. 1-2, pp. 115–126, 2005.

[24] D. K. W. Tang, K. M. Lee, and C. W. W. Ng, "Stress paths around a 3-D numerically simulated NATM tunnel in stiff clay," in *Proceedings of the International Symposium on Geotechnical Aspects of Underground Construction in Soft Ground (IS-Tokyo 99)*, Tokyo, Japan, July 2000.

[25] L. H. I. Meyer, D. Stead, and J. S. Coggan, "Three dimensional modelling of the effects of high horizontal stress on underground excavation stability," in *Proceedings of the International Society for Rock Mechanics and Rock Engineering*, pp. 25–28, Paris, France, August 1999.

[26] R. E. Ranken and J. Ghaboussi, "Tunnel design considerations: analysis of stresses and deformations around advancing tunnels," Final Report to Federal Railroad Administration (Report No. FRAOR & D 75–84), Department of Transportation, Washington, DC. USA, 1975.

[27] G. Hocking, "Three-dimensional elastic stress distribution around the flat end of a cylindrical cavity," *International Journal of Rock Mechanics and Mining Sciences & Geomechanics Abstracts*, vol. 13, no. 12, pp. 331–337, 1976.

[28] Q. S. Xu, Y. Z. Niu, and Q. Z. Li, "Study on construction mechanics of eccentric tunnel method of double-arch tunnel section of Shenzhen metro line 8," *Highway*, vol. 3, pp. 256–259, 2017.

[29] JTG/TF60-2009, "Technical Specifications for Highway Tunnel Construction," China Communications Press, Beijing, China, 2009.